THE JOURNAL OF PHYSICAL CHEMISTRY LETTERS
A JOURNAL OF THE AMERICAN CHEMICAL SOCIETY

pubs.acs.org/JPCL

Letter

Revealing Conformational Transition Dynamics of Photosynthetic Proteins in Single-Molecule Electrical Circuits

Zhiheng Yang,[†] Chenhui Qi,[†] Wenzhe Liu, Dongbao Yin, Longjiang Yu,* Lidong Li,* and Xuefeng Guo*

Cite This: *J. Phys. Chem. Lett.* 2021, 12, 3853−3859

Read Online

ACCESS | Metrics & More | Article Recommendations | Supporting Information

ABSTRACT: The function of proteins depends on their structural flexibility and conformational change. By utilizing silicon-nanowire-based single-molecule electrical circuits, here we present a label-free real-time measurement method that can directly monitor conformational changes of a photosynthetic LH1-RC complex, reaching the ultimate goal of analytic chemistry. These results manifest that the conformation of the LH1-RC complex vibrates among four conformations with strong temperature dependence. At the optimal temperature, States 2 and 3 occupy the main conformations of the LH1-RC complex, and its conformational variation mostly emerges as anharmonic vibration modes, which contributes to photon acquisition and heat transmission. The influence of light activation on occurrence percentage is observed, resulting from light-driven quivering of pigments. Therefore, this avenue proves to be an efficient platform for revealing the fundamental mechanisms of various biological processes *in vitro*.

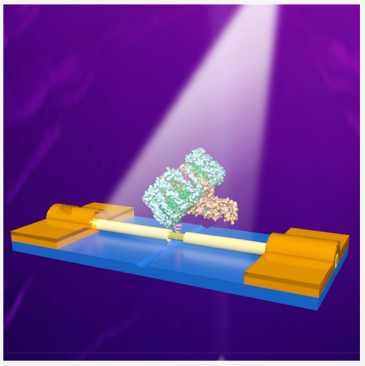

Millions of proteins in humans and other organisms, like strings on a violin or pipes in an organ, vibrate all the time in different ways. These tiny vibrations allow proteins to change their shape quickly so that they can easily interact with other molecules or absorb energy.[1] More meaningfully, the vast biological processes rely on the dynamic structural changes of proteins, such as enzymatic degradation, immune response, and molecular transport.[2] Therefore, to accurately evaluate the structural traits and capture intermediate conformations along with the entire conformational transition pathway becomes necessary to understand these biological processes. However, there remain rigorous challenges for both experimental and theoretical methods, because the main information received by most of the current experimental techniques is ensemble average results covering the behaviors of individual molecules. The method that can record the unabridged dynamic process of the biochemical function is urgent to develop.

Over the past decades, as a robust and profound platform for probing molecular activities of kinetics and thermodynamics, the single-molecule detection methods, based on optical and mechanical strategies including surface plasmon resonance,[3] usage of optical tweezers,[4] fluorescence resonance energy transfer,[5] fluorescence correlation spectroscopy (FCS),[6] microcavity biosensing,[5] and scanning probe microscopy (SPM)[7,8] have been extensively committed to characterize various chemical and biological processes. Recently, it is worthy to mention that single-molecule detection methods have been gradually employed for research into the activity of biological enzymes, gene sequencing and expression,[9] the antibody fixation process, and so on,[10−13] thus affording numerous groundbreaking achievements in biochemistry and biology. Apart from these routine methods, single-molecule electrical detection is particularly attractive because of the realization of direct detection of a molecule, real-time monitoring for a complete process of a molecular reaction, label-free detection without fluorescent pollution/bleaching, and high temporal resolution.[14,15]

One-dimensional (1D) silicon nanowires (SiNWs) exhibit natural compatibility with biological proteins in size and property.[16] What is more significant is that the conductance of SiNWs can be accurately regulated by the periphery charge density in real time. Taking these into consideration, we have developed a new type of high-gain SiNW field-effect transistor (FET)-based biosensor by integrating SiNWs into electrical nanocircuits as perceptual probes.[17] *R. castenholzii* is a thermophilic chlorosome-lacking filamentous anoxygenic phototroph containing the type II pheophytin-quinone RC and light-harvesting antenna complex to form the LH1-RC core complex, which is similar to that of purple bacteria.[18,19] Among most kinds of phototrophic bacteria, there are no cysteine residues located in the light-harvesting complexes, neither the inner α- nor the outer β-polypeptide.[20] However,

Received: March 19, 2021
Accepted: April 12, 2021
Published: April 15, 2021

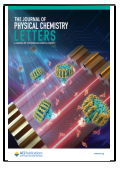

https://doi.org/10.1021/acs.jpclett.1c00884
J. Phys. Chem. Lett. 2021, 12, 3853−3859

the cysteine residue is essential to connect the protein molecule on SiNWs. Therefore, the cysteine-containing outer β-polypeptide of *R. castenholzii* makes it a promising sample for this research. In this work, serving as a local gate, a single LH1-RC complex of *R. castenholzii* was embellished upon SiNWs inside the biosensor. By taking advantage of such a single-molecule electrical detection methodology, the intrinsic activities of the LH1-RC complex have been recorded at the single-event level. These measurements revealed four-level current oscillations in temperatures ranging from 15 to 55 °C, indicating a thermally activated dynamical structural vibration of LH1-RC complexes.[21] These results highlight that SiNW FET-based biosensors may provide a new approach to explore the dynamic conformational changes of bioproteins in the processes such as gene expression, regulation, and modification.

The detailed method of how to fabricate SiNW FET-based single-molecule biosensors (Figures 1a and S1−S4) was

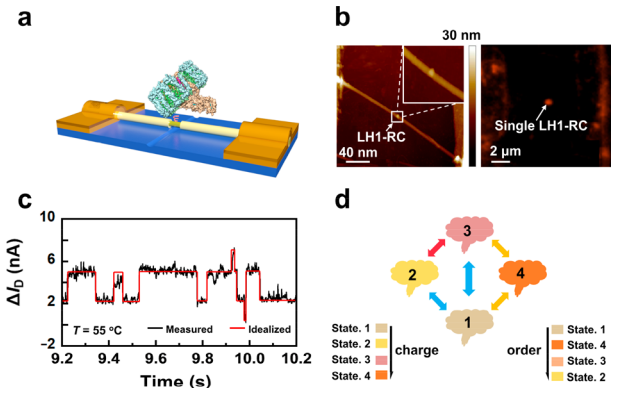

Figure 1. Device characterization and measurements. (a) Schematic diagram of a single-LH1-RC-decorated SiNW biosensor. (b) AFM and STORM images of LH1-RC-decorated SiNWs, where a single LH1-RC complex is attached to the sidewall. (c) Real-time current recordings (black) of 1 s measured in a PBS solution at T = 55 °C and idealized data fitted by QUB software (red). (d) Conversion relationship of four states. Graph of the left bottom is ranked by electric surface charge (charge) and graph of the right bottom is ranked by degree of order (order).

precisely described in our previous work.[22] In brief, the bare device was coated with a poly(methyl methacrylate) layer. Through precise high-resolution electron-beam lithography and HF etching, the 1D Si/SiO_2 core−shell SiNW was opened with a ∼10 nm nanogap, suitable for a single protein in size. Afterward, the protein of interest was assembled into the nanogap and covalently bonded on the sidewall of SiNWs consecutively through alkyne hydrosilylation of Si−H bonds with undecynic acid, *N*-hydroxysuccinimide (NHS) esterification, and a maleimide-Michael reaction. To prove the reliability of point modification, the surface morphology of the resulted device was characterized by atomic force microscopy (AFM) (Figure 1b, left). To further ensure the successful attachment of a single LH1-RC complex on the surface of a SiNW, we also detected the fluorescence signal of the device by stochastic optical reconstruction microscopy (STORM) stimulated with infrared light after electrical measurements (Figure 1b, right). Only a single LH1-RC complex (∼11.5 nm) was observed on the surface of the SiNW (∼17.7 nm), which intactly spans between the source and drain electrodes, thus demonstrating that a single mono-LH1-RC complex had been successfully immobilized on the surface of a SiNW.

To manifest that the current pulses stem from the intrinsic activity of LH1-RC, before decoration with the LH1-RC complex in PBS, a naked SiNW FET device modified with a molecular bridge was detected under the same conditions. Control experiments proved that $I-t$ measurements have thermal dependence and no particular fluctuations with only a Gaussian distribution that is dominated by $1/f$ noise (Figure S5). In the meantime, these results eliminate the possibility of nonspecific surface absorption of either protein or ions in the electrolytic solution on the surface of SiNWs. Then, after immobilization of the LH1-RC complex, we performed the same measurements under the same conditions (bias voltage: 0.3 V; temperature: 55 °C; Tris-HCl buffer pH: 7.8; sampling rate: 57.6 KSa/s). $I-t$ measurements displayed distinct four-level current oscillations at 55 °C (Figure 1c). To verify the liability and efficiency of this observation, we repeated measurements on other devices under the same conditions. The fluctuation of four conductance states reappeared (Figures S6 and S7), proving the reproducibility.

We further carried out systematic measurements in the dark and under light illumination, respectively. It is clear that real-time current recordings exhibit a large-amplitude four-level fluctuation (Figures 2 and 3), again indicating that the conformation of LH1-RC complexes mainly vibrates among four states at 15 °C. The conductance distribution is well-fitted into four Gaussian peaks centered at ∼0.9, ∼2.9, ∼4.5, and ∼7.1 nA, respectively. To better analyze the vibration of current pulses and build the model, four conductance fluctuations are discretely defined as State 1, State 2, State 3, and State 4 from low to high. According to the isoelectric point (pI ≈ 4.6), the LH1-RC complex presents a negative electricity at pH = 7.8. We interpret that the vibration of the LH1-RC complex along with periodic fluctuation of surface charge would induce an alteration of charge transfer and/or a scattering effect derived from the single defect of naked SiNWs, resulting in dynamical stepwise conductance changes of the underlying FET channel. Therefore, the highest current value matches the highest negative electrical state of the LH1-RC complex, and other current values are analogized in order. In summary, four states can be sequenced as State 4 > State 3 > State 2 > State 1, depending on the extent of the negative electrical charge.

For thermophilic bacteria, the temperature plays a key role in the influence on the activity of *R. castenholzii*. To further explore the temperature dependence of LH1-RC, we had measured other four different temperatures (25, 35, 45, and 55 °C) with a 10 °C temperature interval in the dark and under light illumination (Figures 2 and 3). Consistently, we observed that the real-time current trajectories at 15 °C and other temperatures have a uniform four-level conductance distribution (Figures S8 and S9). Tables 1 and S1 show the average dwell times (τ), occurrence percentages of four states (α), and thermodynamic constants (k) of four states at different temperatures. α is obtained by the following formula

$$a_n = \mathrm{A}_n / \sum_i^4 \mathrm{A}_i$$

where n is signed as States 1−4 and A represents the peak area in the current histograms. At 15 °C, α_1 is the maximal lifetime proportion, suggesting that State 1 is the main conformation at

https://doi.org/10.1021/acs.jpclett.1c00884
J. Phys. Chem. Lett. 2021, 12, 3853−3859

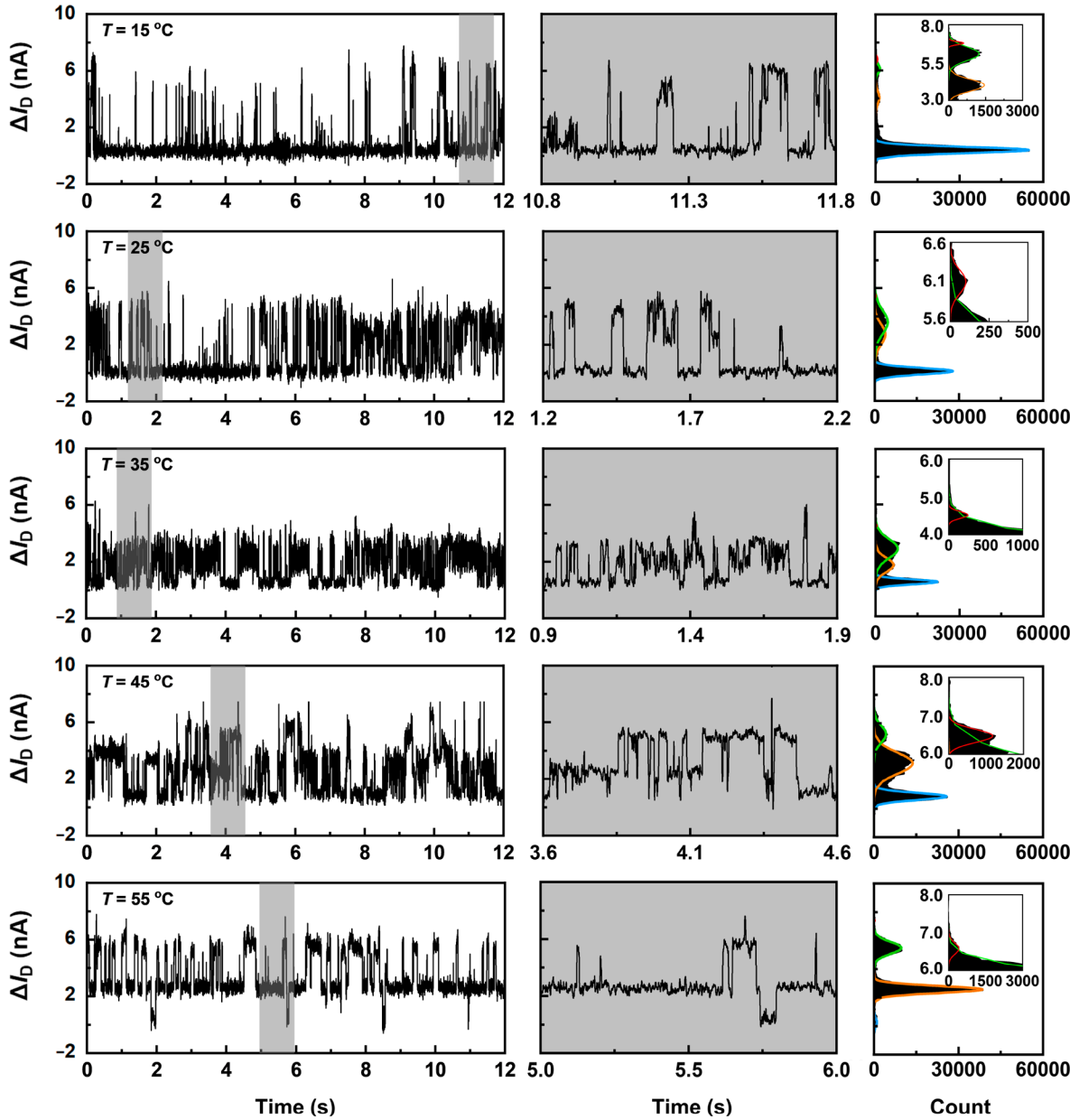

Figure 2. Temperature dependence of the LH1-RC complex vibration in the dark. These graphs show time-averaged data sets of a representative LH1-RC complex vibration measured in a PBS buffer solution in the dark at five different temperatures varying from 15 to 55 °C. The left graphs are real-time current recordings for a duration of 12 s. The middle graphs are amplified 1 s data. The right graphs are the corresponding current histograms.

Table 1. Ocurrence Percentages, and Thermodynamic Constants of Four States in the Dark and under Light Illumination at Different Temperatures

	state	1		2		3		4	
T	parameter	α (%)	k (S^{-1})	α (%)	k (S^{-1})	α (%)	k (S^{-1})	α (%)	k (S^{-1})
15 °C	dark	**91.02**	17.84 ± 0.56	**4.62**	261.78 ± 15.13	**3.60**	58.68 ± 0.21	**0.76**	564.97 ± 28.80
	light	**70.05**	20.45 ± 0.47	**17.18**	226.24 ± 14.39	**12.10**	51.60 ± 0.61	**0.67**	1010.10 ± 113.64
25 °C	dark	**65.04**	20.55 ± 0.37	**14.15**	194.55 ± 4.92	**20.79**	63.41 ± 0.88	**0.02**	571.43 ± 29.46
	light	**48.91**	33.49 ± 0.97	**20.84**	186.92 ± 3.14	**30.04**	62.30 ± 0.82	**0.21**	735.29 ± 76.50
35 °C	dark	**31.55**	66.71 ± 3.52	**25.41**	162.34 ± 2.90	**42.87**	97.46 ± 0.95	**0.17**	819.67 ± 116.48
	light	**21.42**	69.69 ± 3.31	**28.33**	150.38 ± 2.04	**50.07**	93.98 ± 0.62	**0.18**	917.43 ± 67.70
45 °C	dark	**33.28**	65.15 ± 7.04	**53.29**	85.03 ± 1.88	**13.35**	60.35 ± 1.53	**0.08**	1030.93 ± 234.16
	light	**31.54**	67.20 ± 2.58	**54.74**	98.72 ± 3.68	**13.61**	59.70 ± 1.17	**0.11**	1063.82 ± 126.22
55 °C	dark	**2.28**	76.98 ± 9.13	**68.13**	26.27 ± 1.04	**29.53**	35.28 ± 0.83	**0.06**	1052.63 ± 100.62
	light	**2.58**	83.68 ± 10.12	**67.45**	27.26 ± 1.05	**29.90**	33.62 ± 0.05	**0.07**	934.58 ± 174.12

https://doi.org/10.1021/acs.jpclett.1c00884
J. Phys. Chem. Lett. 2021, 12, 3853−3859

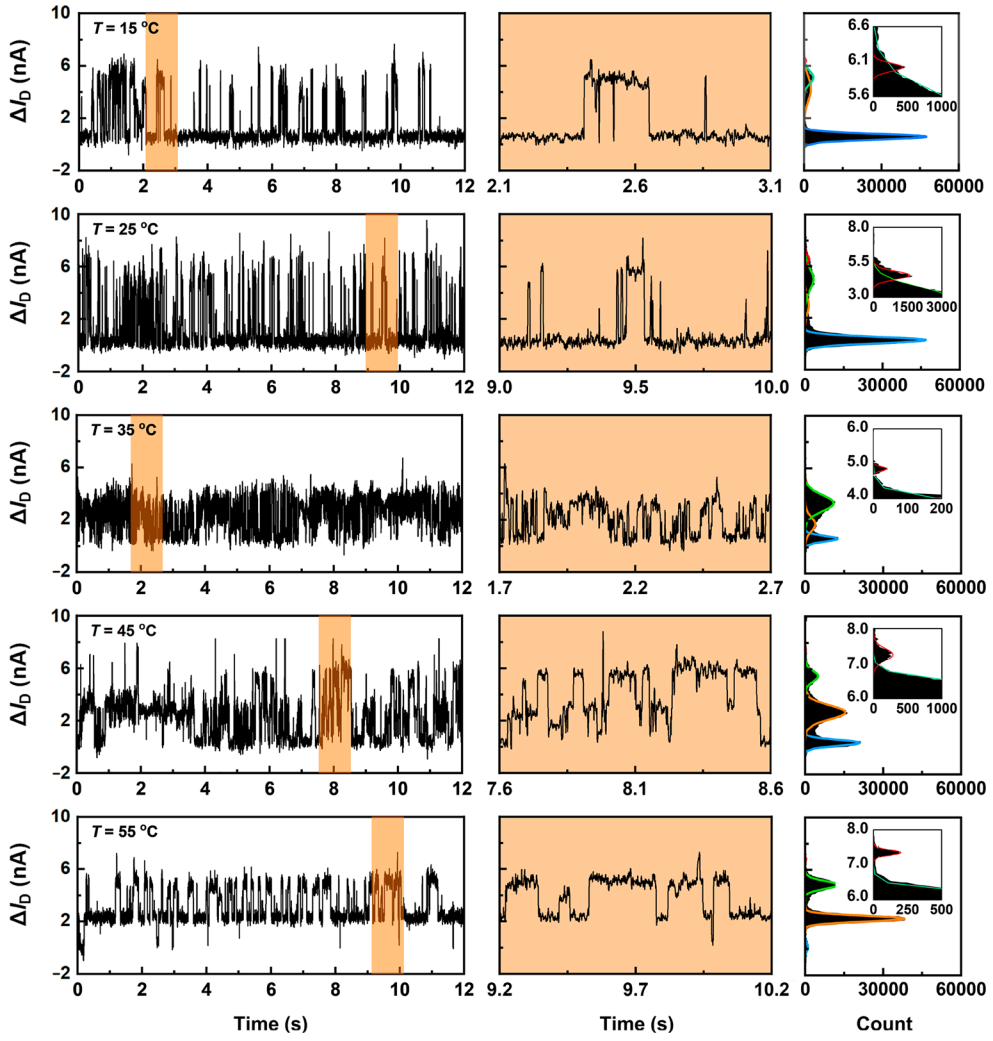

Figure 3. Temperature dependence of the LH1-RC complex vibration under light illumination (wavelength: 400−750 nm; intensity: 100 Lux). These graphs show time-averaged data sets of a representative LH1-RC complex vibration measured in a PBS buffer solution under light illumination at five different temperatures varying from 15 to 55 °C. The left graphs are real-time current recordings for a duration of 12 s. The middle graphs are amplified 1 s data. The right graphs are the corresponding current histograms.

the low temperature. τ_1 is the longest dwell time, while it gradually decreases with increasing temperature, indicating the stability of State 1 changes with the temperature. In contrast to State 1, α_2 becomes the maximal lifetime proportion at 55 °C, representing that State 2 dominates the conformation at this optimal temperature. τ_2 keeps an increase along with the increase of temperature, which indicates that the stability of State 2 is also affected by temperature. However, it is interesting to find that τ_3 reduces against the increasing temperature before 35 °C, but once the temperature reaches 35 °C, the trend turns around unexpectedly. At 55 °C, the optimal temperature to *R. Castenholzii*,[23] τ_3 reaches the peak value of the dwell time, whereas α_3 shows a maximal occurrence percentage at 35 °C. It is proposed that State 3 is also a prominent conformation, which can be activated by the proper temperature and is stabler at 55 °C. The dwell time and occurrence percentage of State 4, in general, is the shortest one, showing that State 4 is an unstable conformation. The assumption is clearly confirmed (Figures 2−4), where States 3 and 2 dominate the conformation of the LH1-RC complex at 55 °C as the mean lifetimes and occurrence percentage of each state display a sequence of $\tau_2 > \tau_3 > \tau_1 > \tau_4$ and $\alpha_2 > \alpha_3 > \alpha_1 >$

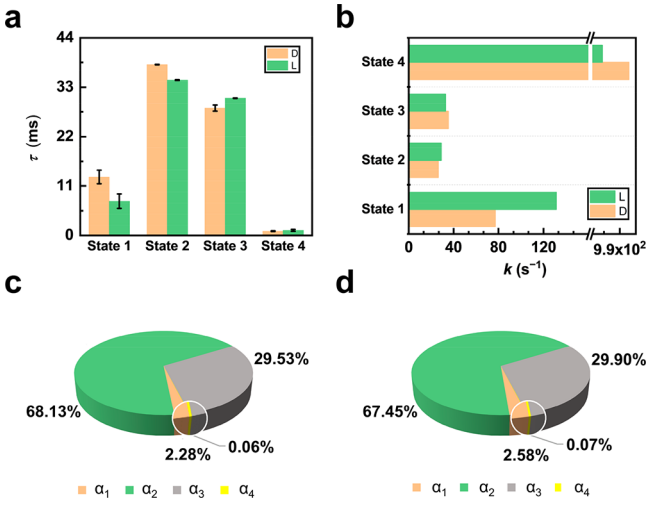

Figure 4. Kinetic analysis. (a) Dwell-time histogram of four states at 55 °C. (b) *k* histogram of four states at 55 °C. (c) Pie chart of four states at 55 °C in the dark. (d) Pie chart of four states at 55 °C under light illumination.

https://doi.org/10.1021/acs.jpclett.1c00884
J. Phys. Chem. Lett. 2021, 12, 3853−3859

α_4. According to the acoustical modes proposed by Nicolai and Delarue, bioproteins are considered as nanoparticles, and all vibration modes with frequencies less than 300 GHz (230 cm^{-1}) are collective modes.[24]

Therefore, we speculate that both States 2 and 3 belong to the protein conformations with higher energy and are predominant conformations of LH1-RC complexes at the optimal temperature, which might be better for LH1-RC to perform physiological functions; State 1 dominates the conformation at low temperatures, State 4 is an ephemeral conformation, and the conformational changes between them frequently occur in these measurements. In addition, the collective vibration of LH1-RC complexes exhibits anharmonic modes under these conditions.

To further investigate the optical dependence of LH1-RC complexes, we simultaneously analyzed the kinetic parameters of the same device in the dark and under light illumination (Tables 1 and S1). In comparison to the case in the dark, only at 15 and 25 °C, τ_1 decreases distinctly by light illumination, and other dwell times have no considerable discrepancy. Slightly different from the dwell time, the influence of light on occurrence percentage of four states exhibits heterogeneities. In general, α_1 reveals a reduction, while α_3 and α_2 show an increase before 45 °C, and then, the influence by light vanishes. This indicates that the stability of State 1 may be weakened by light at 15 and 25 °C, and the occurrence percentage of the four states would not be affected by light when the temperature exceeds 45 °C. In these measurements, light would promote the formation of State 2 and State 3 but hinder State 1 below 45 °C. The dwell time and occurrence percentage of State 4 are maintained within the range of 0.8∼2 ms and 0.02∼0.76%. Based on the Frenkel exciton theory, the quivering of pigments stimulated by light can slightly impact the conformation.[25] Therefore, it is proposed that State 2 and State 3 are conformations, which show the light-driven quivering of pigments that slightly affects the charge distribution of the protein. Furthermore, it is speculated that the vibration of the collective mode would be favorable for photon capture and conformation alternating as a function of time belongs to nonharmonic vibration.

In addition to the discussion of four-level mean lifetimes at different temperatures, another direct and convenient processing approach for analyzing the conformation transition of LH1-RC complexes was developed, relying on the transition equilibrium constant K_T between two states according to the formula: $K_T^{i-j} = k_j/k_i$, where k_i and k_j represent the velocity constant of each conformation, defined as $1/\tau$. The k value of any state and K_T between two states are listed in Table 1.

Then, we calculate the thermodynamic parameters based on the thermodynamic relationship, $\Delta G_T = -RT\ln K_T = \Delta H_T - T\Delta S_T$, where ΔH_T is the change of enthalpy, equivalent to the difference of the total bond energy, and ΔS_T is the change of entropy, representing the order degree index of the system. The conversion among four states (Figures 1−3) can be sorted as State 1 to State 2, State 3, and State 4, State 2 to State 3, and State 3 to State 4 (the conversion between State 2 and State 4 is not found) as depicted in Figure 1d. Detailed thermodynamic results are also listed in Table 1. The plot of $R\ln K_T$ as a function of $1000/T$ shows a linear fit (Figure 5a−d), indicating that the transition process follows an Arrhenius-like behavior and is strongly dependent on temperature. Both in the dark and under illumination conditions, the ΔH_T of the transitions from State 1 to State 2 and State 3 and State 4 is positive,

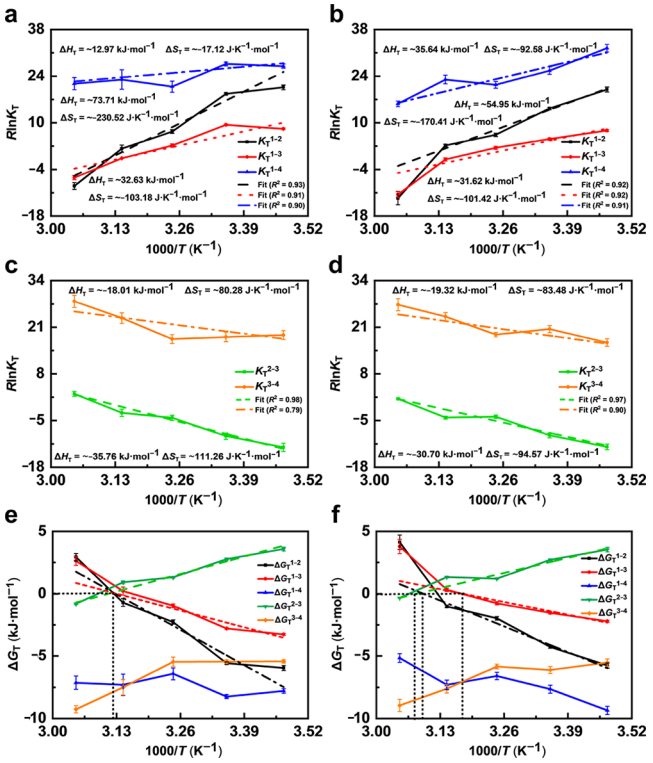

Figure 5. Thermodynamic analysis. (a−d) Plots of $R\ln K$ as a function of $1000/T$ (1−2, black; 1−3, red; 1−4, blue; 2−3, green; 3−4, orange. a and c, in the dark; b and d, under light illumination). (e,f) Plots of Gibbs free energies as a function of $1000/T$ according to the thermodynamic relation (1−2, black; 1−3, red; 1−4, blue; 2−3, green; 3−4, orange. e, in the dark; f, under light illumination). The red plot can be fitted with a line, where the slope is equal to the value of the enthalpy ΔH_T, and the intercept is equal to the entropy ΔS_T.

indicating that the LH1-RC complex transforms from a strong-bonded type to a weak-bonded type. On the contrary, ΔS_T of the transition from State 1 to State 2 and State 3 and State 4 is negative, indicating that the transition of the LH1-RC complex transforms from a disordered state to a well-ordered state (Figure 5a,b). The transitions from both State 2 to State 3 and State 3 to State 4 (Figure 5c) show negative values (∼−35.76 and ∼−18.01 kJ·mol^{-1}) and positive values (∼111.26 and ∼80.28 J·K^{-1}·mol^{-1}).The results signify that the protein conformation transforms from a weak bond energy and well-ordered state to a strong bond energy and disordered state. Furthermore, they have a similar deduction under light illumination (Figure 5d), which means that the conversion is an intrinsic temperature-dependent vibration. In short, the conformations of the LH1-RC complex can be ranked as State 2 < State 3 < State 4 < State 1, based on the degree of disorder. It is worthy to mention that in the dark, ΔG_T^{1-2} and ΔG_T^{1-3} show negative free energies, indicating the spontaneous processes when T is below 46.85 ± 1.76 °C. However, ΔG_T^{2-3} shows negative free energies when T exceeds 46.85 ± 1.76 °C. In other words, only when T exceeds the critical point, the transition from State 2 to State 3 can occur spontaneously. Therefore, this temperature point should be an activation temperature, which leads to the change of the LH1-RC vibration mode. Unexpectedly, it is found that the activation temperature behaves differently under light illumination. Below 41.71 ± 0.89 and 49.81 ± 1.31 °C, the transitions from State 1 to State 3 and from State 1 to State 2

https://doi.org/10.1021/acs.jpclett.1c00884
J. Phys. Chem. Lett. 2021, 12, 3853−3859

are spontaneous. However, beyond 51.31 ± 1.57 °C, only the transition from State 2 to State 3 is spontaneous. In general, the transition from State 1 to State 2 and State 3 is a low-temperature spontaneous process, but the transition from State 2 to State 3 is a spontaneous process at 55 °C, which explains the reason why State 2 and State 3 dominate the main conformation at 55 °C and State 1 dominates the main conformation below 45 °C. Finally, the transitions from State 1 to State 4 and State 3 to State 4 (Figure 5e,f) are spontaneous processes within the temperature range of 15−55 °C.

In summary, we demonstrate an ultrasensitive SiNW FET-based nanosensor capable of realizing a direct, label-free, and real-time electrical detection for revealing the intrinsic dynamic process of an LH1-RC complex at the single-molecule/single-event level. We observed the reproducible large-amplitude four-level current fluctuations, indicating that (1) States 2 and 3 dominate the main conformations at 55 °C; (2) State 1 is a low thermal conformation; (3) State 4 is an unstable conformation; and (4) the stability of four conformations shows strong temperature dependence. The occurrence percentage of the four conformations also reveals strong temperature dependence. Furthermore, photic stimulation can regulate the reversible structural transformational probability between different conformations, thus offering an important step toward better understanding of intrinsic photosynthesis mechanisms. We believe that this unique avenue can be extended to explore the conformation−function relationship of a wide variety of other biosystems under realistic physiological conditions, such as DNA transcription, protein synthesis, and protein structural dynamics.

■ ASSOCIATED CONTENT

Supporting Information

The Supporting Information is available free of charge at https://pubs.acs.org/doi/10.1021/acs.jpclett.1c00884.

Detailed methods of device fabrication; output characteristics for a *p*-type SiNW FET device; process of single-LH1-RC protein decoration; electrical measurement data of a control SiNW device and the reproducibility of another device; statistical analysis of LH1-RC temperature-dependent experiments (PDF)

■ AUTHOR INFORMATION

Corresponding Authors

Lidong Li − *State Key Laboratory for Advanced Metals and Materials, School of Materials Science and Engineering, University of Science and Technology Beijing, Beijing 100083, P. R. China;* orcid.org/0000-0003-0797-2518; Email: lidong@mater.ustb.edu.cn

Xuefeng Guo − *Beijing National Laboratory for Molecular Sciences State Key Laboratory for Structural Chemistry of Unstable and Stable Species, College of Chemistry and Molecular Engineering, Peking University, Beijing 100871, P. R. China;* orcid.org/0000-0001-5723-8528; Email: guoxf@pku.edu.cn

Longjiang Yu − *Photosynthesis Research Center, Key Laboratory of Photobiology, Institute of Botany, Chinese Academy of Sciences, Beijing 100093, P. R. China;* Email: longer@ibcas.ac.cn

Authors

Zhiheng Yang − *State Key Laboratory for Advanced Metals and Materials, School of Materials Science and Engineering, University of Science and Technology Beijing, Beijing 100083, P. R. China*

Chenhui Qi − *Photosynthesis Research Center, Key Laboratory of Photobiology, Institute of Botany, Chinese Academy of Sciences, Beijing 100093, P. R. China*

Wenzhe Liu − *Beijing National Laboratory for Molecular Sciences State Key Laboratory for Structural Chemistry of Unstable and Stable Species, College of Chemistry and Molecular Engineering, Peking University, Beijing 100871, P. R. China*

Dongbao Yin − *State Key Laboratory for Advanced Metals and Materials, School of Materials Science and Engineering, University of Science and Technology Beijing, Beijing 100083, P. R. China*

Complete contact information is available at: https://pubs.acs.org/10.1021/acs.jpclett.1c00884

Author Contributions

†Z.H.Y. and C.H.Q. contributed equally to this work.

Notes

The authors declare no competing financial interest.

■ ACKNOWLEDGMENTS

We acknowledge the primary financial supports from the National Key R&D Program of China (2017YFA0204901 and 2019YFA0904600), the National Natural Science Foundation of China (21727806 and 21933001), and the Tencent Foundation through the XPLORER PRIZE.

■ REFERENCES

(1) Doerr, A. Elusive Vibrations. *Nat. Methods* **2014**, *11*, 226−227.

(2) Havsteen, B. H. Dynamic Analysis of the Atomic Vibrations of Proteins, as Exemplified by the Binding of Myristic Acid to Human Serum Albumin. *Eur. Biophys. J.* **2009**, *38*, 1029−1034.

(3) Halpern, A. R.; Wood, J. B.; Wang, Y.; Corn, R. M. Single-Nanoparticle Near-Infrared Surface Plasmon Resonance Microscopy for Real-Time Measurements of DNA Hybridization Adsorption. *ACS Nano* **2014**, *8*, 1022−1030.

(4) Bustamante, C.; Bryant, Z.; Smith, S. B. Years of Tension: Single-Molecule DNA Mechanics. *Nature* **2003**, *421*, 423−427.

(5) Baaske, M. D.; Foreman, M. R.; Vollmer, F. Single-Molecule Nucleic Acid Interactions Monitored on a Label-Free Microcavity Biosensor Platform. *Nat. Nanotechnol.* **2014**, *9*, 933−939.

(6) Gunther, J. P.; Borsch, M.; Fischer, P. Diffusion Measurements of Swimming Enzymes with Fluorescence Correlation Spectroscopy. *Acc. Chem. Res.* **2018**, *51*, 1911−1920.

(7) Uchihashi, T.; Iino, R.; Ando, T.; Noji, H. High-Speed Atomic Force Microscopy Reveals Rotary Catalysis of Rotorless F1-ATPase. *Science* **2011**, *333*, 755−758.

(8) Wang, M.; Zhang, D. Q.; Zhang, G. X.; Tang, Y. L.; Wang, S.; Zhu, D. B. Fluorescence Turn-on Detection of DNA and Label-Free Fluorescence Nuclease Assay Based on the Aggregation-Induced Emission of Silole. *Anal. Chem.* **2008**, *80*, 6443−6448.

(9) Yan, H.; Xu, B. Q. Towards Rapid DNA Sequencing: Detecting Single-Stranded DNA with a Solid-State Nanopore. *Small* **2006**, *2*, 310−312.

(10) Xin, N.; Guan, J. X.; Zhou, C. G.; Chen, X. J. N.; Gu, C. H.; Li, Y.; Ratner, M. A.; Nitzan, A.; Stoddart, J. F.; Guo, X. F. Concepts in the Design and Engineering of Single-Molecule Electronic Devices. *Nat. Rev. Phys.* **2019**, *1*, 211−230.

(11) Jia, C. C.; Ma, B. J.; Xin, N.; Guo, X. F. Carbon Electrode-Molecule Junctions: A Reliable Platform for Molecular Electronics. *Acc. Chem. Res.* **2015**, *48*, 2565−2575.
(12) Xiang, D.; Wang, X. L.; Jia, C. C.; Lee, T.; Guo, X. F. Molecular-Scale Electronics: From Concept to Function. *Chem. Rev.* **2016**, *116*, 4318−4440.
(13) Li, Y.; Yang, C.; Guo, X. F. Single-Molecule Electrical Detection: A Promising Route toward the Fundamental Limits of Chemistry and Life Science. *Acc. Chem. Res.* **2020**, *53*, 159−169.
(14) Kosuri, P.; Altheimer, B. D.; Dai, M. J.; Yin, P.; Zhuang, X. W. Rotation Tracking of Genome-Processing Enzymes using DNA Origami Rotors. *Nature* **2019**, *572*, 136−140.
(15) Tamaki, T.; Minode, K.; Numai, Y.; Ohto, T.; Yamada, R.; Masai, H.; Tada, H.; Terao, J. Mechanical Switching of Current-Voltage Characteristics in Spiropyran Single-Molecule Junctions. *Nanoscale* **2020**, *12*, 7527−7531.
(16) Wang, Y. L.; Wang, T. Y.; Da, P. M.; Xu, M.; Wu, H.; Zheng, G. F. Silicon Nanowires for Biosensing, Energy Storage, and Conversion. *Adv. Mater.* **2013**, *25*, 5177−5195.
(17) Wang, J. D.; Shen, F. X.; Wang, Z. X.; He, G.; Qin, J. W.; Cheng, N. Y.; Yao, M. S.; Li, L. D.; Guo, X. F. Point Decoration of Silicon Nanowires: An Approach Toward Single-Molecule Electrical Detection. *Angew. Chem., Int. Ed.* **2014**, *53*, 5038−5043.
(18) Collins, A. M.; Kirmaier, C.; Holten, D.; Blankenship, R. E. Kinetics and Energetics of Electron Transfer in Reaction Centers of the Photosynthetic Bacterium Roseiflexus Castenholzii. *Biochim. Biophys. Acta, Bioenerg.* **2011**, *1807*, 262−269.
(19) Collins, A. M.; Xin, Y. Y.; Blankenship, R. E. Pigment Organization in the Photosynthetic Apparatus of Roseiflexus Castenholzii. *Biochim. Biophys. Acta, Bioenerg.* **2009**, *1787*, 1050−1056.
(20) Rucker, O.; Kohler, A.; Behammer, B.; Sichau, K.; Overmann, J. Puf Operon Sequences and Inferred Structures of Light-Harvesting Complexes of Three Closely Related Chromatiaceae Exhibiting Different Absorption Characteristics. *Arch. Microbiol.* **2012**, *194*, 123−134.
(21) Lorenz-Fonfria, V. A.; Furutani, Y.; Ota, T.; Ido, K.; Kandori, H. Protein Fluctuations as the Possible Origin of the Thermal Activation of Rod Photoreceptors in the Dark. *J. Am. Chem. Soc.* **2010**, *132*, 5693−5703.
(22) He, G.; Li, J.; Ci, H. N.; Qi, C. M.; Guo, X. F. Direct Measurement of Single-Molecule DNA Hybridization Dynamics with Single-Base Resolution. *Angew. Chem., Int. Ed.* **2016**, *55*, 9036−9040.
(23) Hanada, S.; Takaichi, S.; Matsuura, K.; Nakamura, K. Roseiflexus Castenholzii Gen. Nov., Sp. Nov., a Thermophilic, Filamentous, Photosynthetic Bacterium that Lacks Chlorosomes. *Int. J. Syst. Evol. Microbiol.* **2002**, *52*, 187−193.
(24) Nicolai, A.; Delarue, P.; Senet, P. Theoretical Insights into Sub-Terahertz Acoustic Vibrations of Proteins Measured in Single-Molecule Experiments. *J. Phys. Chem. Lett.* **2016**, *7*, 5128−5136.
(25) Rancova, O.; Abramavicius, D. Static and Dynamic Disorder in Bacterial Light-Harvesting Complex LH2: A 2DES Simulation Study. *J. Phys. Chem. B* **2014**, *118*, 7533−7540.

https://doi.org/10.1021/acs.jpclett.1c00884
J. Phys. Chem. Lett. 2021, 12, 3853−3859